Spurious convective organization in simulated squall lines

owing to moist absolutely unstable layers

George H. Bryan

National Center for Atmospheric Research*, Boulder, Colorado

Submitted to *Monthly Weather Review*

28 May 2004

Corresponding Author Address: George H. Bryan
National Center for Atmospheric Research
P.O. Box 3000
Boulder, CO 80307
E-mail: gbryan@ucar.edu

* The National Center for Atmospheric Research is sponsored by the National Science Foundation.

Abstract

A spurious updraft pattern has been documented in some numerical simulations of squall lines. The pattern is notable because of a regular pattern of updrafts and downdrafts having comparable amplitude that are 3-6 grid lengths wide. This study examines the environmental and numerical conditions that lead to this problem. The spurious pattern is found only in simulations of upshear-tilted convective systems. Furthermore, the pattern coincides with deep (2-3 km) and wide (5-20 km) moist absolutely unstable layers (MAULs) – saturated layers of air that are statically unstable. In this physical environment, small-scale perturbations accelerate vertically (upward *and* downward). Necessarily imperfect numerical schemes introduce spurious small-scale perturbations into the MAULs, and these perturbations amplify owing to the unstable stratification. Some techniques are investigated that diffuse the perturbations or minimize their introduction in the statically unstable flow.

1. Introduction

Numerical model simulations of deep, moist convection are used for many purposes. One is to explore possible structures of convective clouds and mesoscale convective complexes. Given the difficulties and expense of gathering detailed observations within deep, precipitating convection, the numerical simulation is often considered an attractive method for testing hypotheses concerning the dynamics of clouds and storms. However, numerical models are ultimately based on approximations. Therefore, the model user must be aware of the limitations of numerical model simulations, and must be able to identify features in model output that may not be physically realistic.

Recently, Takemi and Rotunno (2003, hereafter referred to as TR03) presented results from idealized numerical model simulations of squall lines in an environment without vertical wind shear. They documented vertical velocity fields that they note have an obviously unphysical organization. For example, they showed a regular pattern of convective cells at 3 km above ground. The updrafts and downdrafts were of approximately equal amplitude, were about 3 grid lengths wide, and were repeated for several wavelengths in both the along-line and cross-line directions.

Using a similar numerical model, I found this condition to be easily reproducible (Fig. 1). The numerical model, initial conditions, and configuration of this simulation will be detailed in section 2 of this paper. For the purpose of this introduction, it is sufficient to note that this simulation was conducted with a setup nearly identical to those of other idealized modeling studies, such as Rotunno et al. (1988) and Weisman (1993). That is, a squall line was triggered with a line thermal in a horizontally homogeneous environment using 1 km horizontal grid spacing. Several characteristics of this vertical velocity pattern make it unphysical. The cells are

2-3 grid lengths wide, which is unusually poorly resolved for the grid spacing used. The regular, repeating pattern seems artificial; an unorganized pattern of updrafts is expected in such conditions. Finally, the downdrafts have similar size, shape, and amplitude as the updrafts, which also suggests an artificial organization.

TR03 note that this spurious updraft pattern is paradoxical, given the high-order numerics inherent in their numerical model, a version of the Weather Research and Forecasting (WRF) Model. The formulation of the WRF Model allows it to be used without artificial diffusive terms. Instead, WRF Model simulations typically use a small amount of flow-dependent implicit diffusion that acts primarily on small-scales (e.g., Wicker and Skamarock 2002, TR03). Consequently, results from the WRF Model were expected to contain less numerical errors than results from older codes used in some previous studies.

After further analysis, TR03 conclude that most previous modeling studies had a greater amount of diffusion which probably prevented the appearance of such spurious vertical velocity patterns. This conclusion seems reasonable, given the existence of artificial diffusion terms required to prevent numerical errors from contaminating the solution in leapfrog-in-time models with (relatively) low-order numerical schemes, such as the Klemp–Wilhelmson model (Klemp and Wilhelmson 1978), the Penn State–NCAR Mesoscale Model (MM5; Dudhia 1993), and the Advanced Regional Prediction System (ARPS; Xue et al. 2000).

TR03 addressed the problem through the model's subgrid turbulence scheme. By modifying certain tunable parameters within the turbulence scheme, they were able to obtain more reasonable looking results (e.g., Figs. 4-5 of TR03). In conclusion, they suggested optimum values for these parameters, which they argue are "appropriate for mesoscale cloud simulations" (i.e., simulations with horizontal grid spacing of order 1 km).

It is clear, given the simulations presented by TR03, that increasing the diffusiveness of a numerical model will damp the spurious updraft pattern, and that the results with more diffusion are better than the original results. It is also reasonable to argue that the proposed method if increasing diffusion – i.e., via the subgrid turbulence scheme – is preferable to adding an artificial diffusion term, which acts to diffuse every small-scale perturbation throughout the domain, regardless of local environmental conditions (such as Richardson number). Thus, the most important conclusions of TR03 are not addressed by this new study.

However, it seems that the ultimate cause of the spurious updraft pattern was never established by TR03. It is possible that the cause of the spurious organization still remains in their simulations, but that the effects (i.e., spurious updraft patterns) are merely damped by the additional diffusivity of the model. A proper identification of the cause of the problem may lead to a better solution to the problem, which would then allow one to determine appropriate settings for other model components (such as values for turbulence parameters).

This paper is intended as a follow-up to the study of TR03. New insight is added based on simulations not conducted by TR03. Additionally, an explanation is offered concerning the cause of the spurious updraft pattern and concerning the methods one can use to prevent it from becoming a problem.

Ultimately, this new study suffers from the same limitation as that of TR03: the reliance on qualitative assessments. The absence of a "true" or "correct" solution prevents a conclusive decision on what the best result should be. However, it is hoped that the information provided herein will advance the discussion on model configurations suitable for the simulation of convection in the idealized framework used here.

2. Methodology

The nonhydrostatic numerical model described in Bryan and Fritsch (2002) is used in this study. This model is based on the third-order Runge-Kutta time integration scheme for compressible equations (Wicker and Skamarock 2002). Consequently, the model used here is broadly similar to the height-based vertical coordinate version of the WRF Model used by TR03.

This study uses a "standard" equation set [i.e., equation set "A" of Bryan and Fritsch 2002)], mainly to facilitate comparison with other commonly used numerical models. In this formulation, the thermodynamic and pressure equations were developed assuming that the specific heat of liquid water is zero, and that the diabatic contribution to the pressure equation can be neglected. Thus, the model's governing equations are essentially the same form as those in the Klemp-Wilhelmson model, MM5, and ARPS, among others. Unlike the WRF Model used by TR03, this formulation does not conserve total dry-air mass during the simulation.

To be consistent with TR03, the horizontal advection is fifth-order and the vertical advection is third-order, based on the formulation provided by Wicker and Skamarock (2002). Also, the subgrid turbulence scheme is nearly identical to that used by TR03, and is based on the turbulence kinetic energy scheme of Deardorff (1980). Unless specified otherwise, the value used for the parameter C_k is 0.10. In all simulations, the value for C_e is 0.93. (The turbulence parameters C_k and C_e are defined in TR03.) As in TR03, the stability dependence on these parameters is removed by specifying a constant length scale, $l = (\Delta x \Delta y \Delta z)^{1/3}$.

The domain is 400 km long in the across-line (i.e., x) direction, 80 km long in the along-line (i.e., y) direction, and is 18 km deep. The domain is longer than that used by TR03 to accommodate a set of simulations in which the domain is not translated. Specifically, the increased length is necessary to keep the convective system inside the domain for all simulations.

In all other aspects, the simulations are configured as in TR03. Open lateral boundary conditions are used in the *x* direction, and periodic boundary conditions are used in the *y* direction. A Rayleigh damping layer is applied over the upper-most 6 km of the domain to minimize wave reflections from the upper boundary. The Kessler (1969) liquid-only microphysics scheme is used, the Coriolis parameter is zero, no atmospheric radiation scheme is used, and no surface fluxes or surface friction are applied. The horizontal grid spacing is 1 km, the vertical grid spacing is 500 m, the large time step is 6 s, and the small time step is 1.5 s. The simulations extend 4 h in time.

The initial thermodynamic conditions are horizontally homogeneous, based on the analytic sounding of Weisman and Klemp (1982) (Fig. 2a). A squall line is initiated by using a line thermal that has infinite size in the *y* direction, a 10 km radius in the *x* direction, a 1.5 km radius in the *z* direction, and a maximum potential temperature perturbation of 1.5 K at its center. Random potential temperature perturbations of maximum amplitude 0.1 K are inserted throughout the line thermal to allow three-dimensional structure to develop.

Four environmental wind profiles are studied, where only the low-level shear oriented perpendicular to the squall line is varied (Fig. 2b). The environmental conditions will be referred to by the magnitude of wind variation over the lowest 2.5 km (U_s), as indicated at the top of Fig. 2b. For the initial (i.e., "control") simulations, a mean wind speed is subtracted from the initial wind profile to keep the squall line roughly in the middle of the domain during the entire simulation.

As in TR03, vertical velocity spectra are computed from the model output to quantify details of the spurious updraft pattern. The spectra are computed over an 80 x 80 km^2 subdomain extending roughly 20 km ahead of the surface gust front to about 60 km behind the gust front. In

contrast to TR03, here a two-dimensional Fourier transform is performed. The results are presented one-dimensionally by averaging the two-dimensional spectrum in the *x* or *y* directions (i.e., in the across-line and along-line directions, respectively). This method allows for a relatively smooth spectral analysis using output from one output time.

Parcel trajectories were calculated during the model simulation to allow an assessment of conditions in a parcel-relative framework. To optimize accuracy of the calculations, the parcels were translated every time step during the model simulation. Environmental conditions were interpolated to the parcel position to evaluate the conditions experienced by the parcels as they pass through the convective region of the squall lines.

3. Dependence on environmental shear

One general conclusion of this study is that the spurious updraft pattern only occurs in certain environments (Fig. 3). As found by TR03, the simulation with no environmental shear contains obviously spurious organization (Fig. 3a). The dominant wavelength of the vertical velocity pattern is about 3Δ in both the *x* direction and *y* directions, where Δ refers to the horizontal grid spacing. For $U_s = 10$ m s^{-1}, an unphysical pattern is still present (Fig. 3b); in this case, the updrafts and downdrafts in the across-line (i.e., *x*) direction have a wavelength of roughly 6Δ, but there is comparatively less variation in the along-line (i.e., *y*) direction.

For larger low-level shear, a spurious pattern is not apparent. In the $U_s = 20$ m s^{-1} simulation, the low-level updraft is closer to the surface gust front and is nearly continuous along the line (Fig. 3c). A few, weak updrafts exist several km behind the line, but there is no evidence of a regular pattern of poorly resolved cells. Similarly, the $U_s = 30$ m s^{-1} simulation does not show any obvious signs of an unphysical pattern, but instead could be characterized as a series of

well-resolved cells along the line (Fig. 3d). The model output was checked at other levels and at different times, and no obvious evidence for a spurious updraft pattern was discovered in these two larger-shear runs.

TR03 also found that the spurious pattern was not apparent in an environment with U_s = 20 m s^{-1}. Their explanation for the lack of a problem in this environment was based on the implicit diffusion within the fifth-order advection scheme. For this scheme, the amount of diffusion is proportional to the grid-relative advective wind speed. Therefore, the U_s = 0 m s^{-1} simulation should have small implicit diffusion owing to small wind speeds, while the U_s = 20 m s^{-1} would have more diffusion owing to the higher wind speeds. Thus, TR03 conclude that the spurious pattern is suppressed by the greater implicit diffusion.

Although this explanation seems plausible, there is evidence that increased diffusion is not the reason why the spurious organization does not occur in larger-shear environments. Using the same model configuration, I conducted an additional set of simulations in which a different mean wind was subtracted from the initial wind profile (hereafter referred to as the "shifted-wind" simulations). The goal in these simulations was to have zero mean grid-relative horizontal flow in the region where the spurious updrafts are found, i.e., at roughly the 3 km level and near the cold pool head. Thus, the goal was to *decrease* the amount of implicit diffusion in all runs, and furthermore to have a comparable amount of diffusion between runs with different shears. To keep the squall line inside the domain during the entire simulation, the initial line thermal was moved from the center of the domain to a location west of center. Thus, in these simulations the squall line moves several hundred km eastward, as opposed to the control simulations in which the squall line remains near the center of the domain at all times. Because no surface friction is included in the simulations, the two results should be identical, owing to Galilean invariance. Of

course, some differences are expected for numerical reasons, but these differences should be minor; however, it will be shown shortly that this is not the case.

To establish the magnitude of diffusion in the "control" and "shifted-wind" simulations, an estimate for the diffusion coefficient in the region of interest is presented based on line-averaged values of horizontal wind, *u*. This variable was calculated at 3 km above ground and in the region where updrafts occur; this location for the four shears is 10, 5, 2, and 0 km behind the surface gust front for the U_s = 0, 10, 20, and 30 m s^{-1} cases, respectively. The horizontal diffusion coefficient, α, implied by the *u* values is

$$\alpha = \frac{|u|}{60\Delta x} \qquad (1)$$

(Wicker and Skamarock 2002). Table 1 lists the results for the "control" and "shifted-wind" simulations. These results suggest that the simulation with the greatest amount of diffusion in the "control" simulations was the U_s = 10 m s^{-1} case. This simulation had an apparent spurious organization, despite having the largest implicit diffusion. The U_s = 20 m s^{-1} had a comparable amount of diffusion, yet has an apparently acceptable solution. Interestingly, the U_s = 30 m s^{-1} case had the least amount of diffusion at 3 km, despite having a qualitatively acceptable solution. As designed, the "shifted-wind" simulations have less diffusion compared to the "control" simulations, and roughly similar diffusion among shear environments (Table 1).

Although the results should be similar, the patterns of *w* in the "shifted-wind" simulations are markedly different from the "control" results – and not in the manner that one might expect, considering the lower implicit diffusion. For the U_s = 0 and 10 m s^{-1} runs, the spurious updraft patterns have been eliminated (Figs. 4a and 4b). The updrafts in the U_s = 0 m s^{-1} case remain

poorly resolved, but two of the spurious characteristics are not present: downdrafts with comparable amplitude to the updrafts; and a regular pattern across and along the line. These spurious characteristics are also absent from the $U_s = 10$ m s^{-1} case (Fig. 4b).

In contrast, the results for $U_s = 20$ and 30 m s^{-1} are qualitatively similar to the patterns in the "control" simulations. The $U_s = 20$ m s^{-1} has long segments of nearly continuous updraft (Fig. 4c), and the $U_s = 30$ m s^{-1} simulation has several well-resolved cells along the line (Fig. 4d). Thus, the Galilean invariance is better captured in the larger shear simulations.

To assist with the interpretation of results, vertical velocity spectra were computed from the fields shown in Figs. 3-4. Because only one output time was used for the computation, the spectra are for only the fields shown in Figs. 3-4, and allow for a quantification of patterns already discussed subjectively. The spectra are displayed in Fig. 5, with the along-line spectra multiplied by 100 to avoid overlap. On all panels, the scale corresponding to 6Δ is highlighted by a vertical line. Recent studies have found that the effective resolution in this model configuration is approximately 6 times the grid spacing (Bryan et al. 2003, Skamarock 2004). Thus, anything to the left of this line in spectra should be interpreted as a physical solution that is unaffected, at least directly, by model diffusion. Anything to the right of this line in spectra is damped directly by the model's diffusion, and should be interpreted as poorly resolved.

The across-line spectrum for the $U_s = 0$ m s^{-1} "control" simulation quantifies the spurious nature of the vertical velocity pattern; a pronounced increase in energy occurs at poorly resolved scales, with a peak at ~3Δ (Fig. 5a). This peak does not occur in the "shifted-wind" simulation, even though less diffusion is implied by the lower horizontal wind speeds at this level. In contrast, the along-line spectra for the two simulations are practically identical at both well resolved and poorly resolved scales.

For the $U_s = 10$ m s^{-1} environment, the "control" simulation also shows a distinct buildup of energy in the across-line direction, but in this case is maximized at 6Δ (Fig. 5b). The sharp increase of energy from 12Δ to 6Δ is suspicious, but is not as obviously problematic as the clearly under-resolved peak in the $U_s = 0$ m s^{-1} case. On the other hand, the "shifted-wind" simulation does not contain such a peak near the model's effective resolution. In fact, the difference in overall across-line spectral structures for the "control" and "shifted-wind" simulations is disturbing, given that the results should be identical, owing to Galilean invariance. For the along-line spectra, the results are broadly similar, especially at scales smaller than 10Δ.

The spectra from the two larger-shear cases do not reveal such distinct differences between simulations. For $U_s = 20$ m s^{-1}, the well-resolved sections of the spectra are nearly identical (Fig. 5c). The only substantial difference occurs at the smallest scales in the along-line spectra, where the "control" run has notably lower energy. The $U_s = 30$ m s^{-1} spectra also have no obviously spurious features, and the spectra from the two runs are qualitatively similar (Fig. 5d).

Although the ultimate cause of the spurious updraft pattern has not been explained yet, it can be concluded that a lack of diffusion is not a candidate. When the implicit flow-dependent diffusion is reduced, the spurious pattern is avoided. Furthermore, the results suggest an environmental dependence that requires explanation; for some reason, the low-shear environments allow the spurious pattern, while the large-shear environments do not. Finally, there is a disturbing difference for results that should be very similar.

4. An explanation for the spurious pattern

To provide better guidance to the numerical modeling community, an explanation for the ultimate cause of the spurious pattern is necessary. If this can be determined, it might be easier to devise solutions to control or prevent the problem.

a. The cause of the spurious oscillations

The conditions in which the spurious updraft pattern exists are highlighted by a vertical cross section from the $U_s = 0$ m s^{-1} "control" simulation (Fig. 6). From a system-relative-flow perspective, the spurious pattern first occurs where the air first becomes saturated – in this case, about 8 km to the east of the surface gust front. This is where subtle, small (2-3 Δ) oscillations appear in the thermodynamic and kinematic fields. As this air ascends over the cold pool, the alternating updraft/downdraft pattern is amplified. Ultimately, the pattern ceases to exist when a more uniform vertical profile of equivalent potential temperature (θ_e) is created, roughly 15 km to the west of the gust front.

In these squall line simulations, the spurious pattern forms, amplifies, and dissipates within deep (~2-3 km) and wide (~5-20 km) moist absolutely unstable layers (MAULs). A MAUL is a layer of air that is saturated and is statically unstable. Typically, these layers appear on a thermodynamic diagram (such as a skew-T) as a saturated layer in which θ_e decreases with height (e.g., Fig. 7). In mesoscale convective systems, a MAUL often forms where an initially unsaturated and conditionally unstable environment is lifted to saturation over a deep layer by the ascent associated with cold pools (Kain and Fritsch 1998; Bryan and Fritsch 2000). This is the same location where the spurious updraft pattern occurs.

Obviously, a MAUL is amenable to immediate convective overturning. In fact, both ascending *and* descending air in a MAUL will accelerate away from their current locations, as long as saturation can be maintained. This probably explains, at least partly, the regular pattern of updrafts and downdrafts; the environmental condition is one in which both updrafts and downdrafts amplify. This might explain why downdraft amplitudes are comparable to updraft amplitudes, as in the spurious *w* patterns of Fig. 1.

However, this analysis does not explain why the spurious pattern has a poorly resolved scale (3-6 Δ), or whether such a pattern is actually physical. Two additional facts help address these points. First, the resolution used for these simulations (Δ = 1 km) is too coarse to adequately represent the processes that probably occur in actual MAULs. If one wanted to resolve explicitly the overturning in a 2 km deep turbulent layer, one would need grid spacing on the order of 100 m (Bryan et al. 2003). With much higher resolution – and in the actual atmosphere – one should expect to see turbulent overturning at a spectrum of scales smaller than 2 km. Large updrafts would probably emerge from this turbulent layer, as in this coarse simulation. However, a regular series of 2-3 km wide updrafts seems unlikely.

Second, the coarse resolution introduces numerous numerical difficulties. Finite difference techniques, such as those used in this numerical model, have difficulties translating poorly resolved features. It is probable that spurious perturbations are being introduced into the MAUL by dispersive errors in the advection scheme. Linear advection tests often reveal these perturbations (e.g., Fig. 1 of Wicker and Skamarock, 2002). The well-known "overshoots" and "undershoots" generated by these schemes naturally damp in a statically stable environment; however, in MAULs they amplify.

To summarize, it is reasonable to conclude that the spurious updraft pattern is ultimately caused by a combination of imperfect numerics and the presence of a statically unstable environment. Thus, it is a combination of a numerical problem and a physical situation that allows the problem to amplify.

This hypothesis is difficult to prove because the use of imperfect numerics is unavoidable. On the other hand, it might be possible to see a trend towards decreasing spurious structures as numerical problems are reduced. For example, one could try using a monotonic advection scheme, which does not introduce spurious overshoots and undershoots. Such a scheme is examined in the following section, and shows some promising results. However, monotonic schemes are implicitly diffusive, especially towards poorly resolved structures. This leaves open the question of whether one is simply adding greater diffusion to the solution by the use of a monotonic scheme.

Another alternative would be to conduct simulations with numerical models that are comparatively free of spurious oscillations. Examples might include spectral or psuedo-spectral models. These squall line simulations could be repeated with such models in future studies, to see if they have an intrinsic advantage over finite-difference-based models.

Although it is difficult to prove that the errors inherent in model numerics are ultimately responsible for the spurious pattern, there is some circumstantial evidence to support the hypothesis. For example, in the $U_s = 0$ m s^{-1} "control" run the updrafts are advected westward during the simulation by the system-generated circulation. A time-space (i.e., Hovmöller) diagram highlights how the cells move with the mean horizontal wind speed in the MAUL: about 5.5 m s^{-1} (Fig. 8). In contrast, in the "shifted-wind" simulations, the initial wind is adjusted so that the horizontal flow on the grid is zero in this layer – and there is no spurious

pattern in these simulations. It can be surmised that because the cells are not advected laterally, there is no introduction of spurious oscillations from the advection scheme. This is a likely explanation for the apparently superior results in the "shifted-wind" simulations, even though the diffusion is lower. That is, if one does not introduce the perturbations, then one does not have to diffuse them.

b. Shear dependence

The shear dependence documented in section 3 can now be explained. Because the spatial properties (e.g., depth and width) of MAULs vary with squall line structure, the spurious overturning problem should only be expected under certain conditions. Analysis of the MAUL properties from the simulations reveals that MAULs are deepest and widest in strongly upshear-tilted convective systems (Fig. 9). For the simulations in this study, this system structure occurs when the low-level shear is weak. There are additional environments, not studied here, that can promote upshear-tilted convective systems, such as strong reverse shear (e.g., the "jet" profiles of Weisman et al. 1988).

The depth and width of the MAUL are not, necessarily, the relevant properties that can lead to spurious updraft patterns. Rather, these are properties that promote long parcel residence time within the MAUL. Sample parcel trajectories for the four control simulations are included in Fig. 9. For the $U_s = 0$ m s^{-1} case (Fig. 9a), parcels ascend as they approach the system's cold pool, but then move nearly horizontally through a MAUL. Not all parcels have a quasi-horizontal trajectory such as that shown in Fig. 9a. In fact, some parcels ascend more rapidly through vertically growing cells. However, quasi-horizontally moving parcels are more common in the upshear-tilted systems, including the $U_s = 10$ m s^{-1} case. In contrast, in the comparatively

more upright system of the U_s = 20 m s^{-1} simulation (Fig. 9c), and in the downshear-tilted U_s = 30 m s^{-1} simulation (Fig. 9d), the parcels typically ascend continuously from low-levels to the upper-troposphere, with less horizontal advection through MAULs. Given that horizontal advection can be a source of small-scale, spurious perturbations, the upshear-tilted systems should be more susceptible to the spurious organizational problem.

Average parcel residence times and horizontal displacement within MAULs are listed in Table 2 for the "control" simulations and in Table 3 for the "shifted-wind" simulations. In general, these data show that parcels spend more time within MAULs in the upshear-tilted systems – i.e., in the lower shear environments. However, there is a subtle difference between results from the two sets of simulations; the residence time trends downward monotonically for the "shifted-wind" simulations, but not for the "control" simulations. Because the "shifted-wind" simulations are not affected by the spurious pattern, these results are probably more realistic. Despite these details, it is clear that parcel residence time within MAULs trends downward as system structure becomes more upright.

The value for horizontal (x) displacement on the grid is dependent on the horizontal grid-relative wind speeds experienced by the parcels. The important point to draw from this analysis is that the horizontal displacement within the MAUL is lower in the "shifted-wind" simulations (Table 3) than in the "control" simulations (Table 2). This result supports the hypothesis from the previous subsection that horizontal advection within MAULs is primarily responsible for the occurrence of the spurious updraft pattern.

These results contribute evidence, combined with theory from the previous subsection, that MAULs are a factor in the development of the spurious updraft pattern. The spurious pattern seems to be most likely for large parcel residence times in MAULs combined with

horizontal grid-relative advection within the MAUL. This explains why the spurious updrafts are most likely in environments that encourage upshear-tilted convective systems, such as weak wind shear.

c. Structural differences

Although the conditions in the $U_s = 0$ and 10 m s^{-1} simulations both favor the formation of spurious updraft patterns, there is clearly a structural difference in the pattern. The $U_s = 0$ m s^{-1} simulation is characterized by comparatively small cells on the order of 3Δ, while the $U_s = 10$ m s^{-1} simulation has a comparatively better resolved wavelength of approximately 6Δ (Figs. 3 and 5). This result is robust; it has been reproduced in several tests with the current model, in which numerical techniques such as advection schemes were varied. Additionally, a model intercomparison has been conducted on similar squall lines with J. Knievel of the National Center for Atmospheric Research and M. Parker of the University of Nebraska-Lincoln. We have found qualitatively similar results for simulations with the WRF Model and with ARPS. All three models used in the intercomparison vary in several ways, from the time integration scheme, to the order of the spatial derivatives used in the advection scheme, to inevitable differences in how one applies physical processes. The fact that the spurious updraft pattern is similar in different models points to an environmental, rather than numerical, dependence to this scale.

The ultimate reason for the differences in spatial scales is possibly related to differences in cold pool structure. For the $U_s = 10$ m s^{-1} case, the ascent at the cold pool head is deeper, stronger, and wider (across the line) than in the $U_s = 0$ m s^{-1} case. Therefore, a deeper and wider layer of high θ_e air ascends at the cold pool head in the $U_s = 10$ m s^{-1} case. Because this

physically-based scale varies with environmental conditions, the subsequent overturning within the MAUL is perturbed at different scales. Ultimately, however, the evidence points to inaccuracies in the advection scheme as the source for spurious perturbations within this otherwise physical flow.

5. Solutions to the problem

One solution to the spurious problem has already been presented. Apparently, one can avoid the problem by minimizing horizontal advection within the MAUL (e.g., the "shifted-wind" simulations, Fig. 4). However, this solution is not generally suitable to all applications. For example, there may be varying low-level shear along the line in some squall lines. This technique also requires a great deal of knowledge about how the system will evolve before the simulation is started. More general solutions are necessary.

The following tests are not comprehensive. There may be solutions other than those presented here, and a variety of parameter settings (such as diffusion coefficients) are not investigated. Furthermore, different numerical modeling systems may be less susceptible to this problem in the first place. The main purpose of this section is to present possible solutions for finite-difference-based models in the context of the explanation offered earlier – i.e., that numerically generated perturbations amplify in a statically unstable environment.

The following simulations were performed for all four shear environments. However, a general conclusion drawn from these studies is that the larger-shear environments are not sensitive to these changes; the same qualitative structure appears in all high-shear runs, and is broadly similar to that is Figs. 3-4. In contrast, the low-shear simulations show a large variation

in results. Thus, to focus the discussion, only the U_s = 0 and 10 m s^{-1} results are shown in this section.

a. Increased turbulence parameters

TR03 recommend increasing diffusion via the model's subgrid turbulence parameterization. Based on a series of simulations, they recommend increasing C_k above its commonly used value of ~0.10, while keeping C_e at 0.93. Following their suggestion, results using C_k = 0.20 in the Bryan-Fritsch model are shown in Fig. 10. As in TR03, the solution is more diffused, and the spurious updraft pattern is not apparent. However, the increased turbulence parameters act to nearly eliminate all updrafts in the U_s = 0 m s^{-1} simulation (Fig. 10a). In contrast, the simulation with U_s = 10 m s^{-1} contains strong cells, without evidence of the spurious pattern (Fig. 10b). The spurious "spikes" in the across-line spectra have been removed by this technique (not shown). However, the large-scale energy in the U_s = 0 m s^{-1} simulation has been severely reduced by this method.

To address whether C_k = 0.20 is too large for this numerical model, a series of simulations was conducted in which C_k was increased in small increments from 0.10 to 0.20. Based on these results, C_k of 0.14 was the minimum value necessary to eliminate the spurious features for U_s = 0 m s^{-1}, but C_k of 0.18 was the minimum necessary for U_s = 10 m s^{-1}. This result, and the fact that the U_s = 20 and 30 m s^{-1} cases do not require an increase of C_k, suggest that simply increasing C_k is not a general solution that will be sufficient for all applications. In fact, there appears to be an environmental dependence to the "optimal" value of C_k, which, again, means that a good deal of knowledge of the simulated results is needed before an appropriate value can be chosen. Furthermore, the "shifted-wind" simulations presented earlier do not show

any obvious need for an increase in C_k in the first place, further raising doubts about the need for increased turbulence parameters.

b. Artificial diffusion

Historically, the inclusion of an artificial diffusion term has been a common method to control small-scale numerical noise. For example, artificial fourth-order diffusion is used in the Klemp-Wilhelmson Model, MM5, and ARPS, to name but a few. A more scale-selective sixth-order diffusion is also used by some modelers (e.g., Carpenter et al. 1998; Lane et al. 2003). Application of artificial sixth-order diffusion would be very effective at removing the 3Δ structures of the $U_s = 0$ m s^{-1} simulation. However, sixth-order diffusion acts primarily on scales less than 6 Δ (e.g., Durran 1999, pg. 84). Therefore, sixth-order diffusion may be ineffective for the $U_s = 10$ m s^{-1} simulation.

It has been argued that the higher accuracy of the advection schemes in the WRF Model, combined with some implicit diffusion inherent in the odd-ordered advection schemes obviates the need for artificial diffusion (TR03). However, given the results presented here, an argument could be made that some artificial diffusion would be prudent.

To test the effect of artificial diffusion, the simulations were repeated with standard fourth- and sixth-order artificial diffusion (as in Durran 1999) applied only horizontally to all variables except pressure. The diffusion coefficient is 4.8% of one-dimensional stability for both schemes; thus, 2Δ structures are damped at the same rate in both schemes. This value for diffusion coefficient is the same as the default value for MM5 and ARPS, and is slightly stronger than the "FILTER1" applied in tests by TR03.

As expected, the solutions with artificial diffusion (Figs. 11 and 12) are generally smoother than the results of the "control" simulation (Fig. 3). Furthermore, the fourth-order scheme clearly acts on scales larger than the sixth-order scheme. Curiously, for the $U_s = 0$ m s^{-1} run, the fourth-order diffusion almost completely eliminates most updrafts (Fig. 11a), whereas the sixth-order diffusion allows many strong updrafts to persist in this environment (Fig. 12a).

Spectra from these simulations (not shown) confirm that the application of standard sixth-order diffusion does not eliminate the problem; the across-line spectrum shows a questionable peak at ~7Δ for both shears. It is tempting to surmise that the diffusion coefficient is not large enough to control the problem in this case. On the other hand, standard fourth- and sixth-order diffusion schemes can introduce spurious small-scale perturbations (e.g., Xue 2000). The hypothesis from the previous section argues that spurious oscillations introduced by numerical schemes is the ultimate cause of the spurious updraft pattern. In this context, the standard diffusion schemes may, in some instances, introduce more problems through their oscillatory nature than they solve through their diffusiveness.

Based on these results, the simulations were repeated using the simple monotonic diffusion scheme of Xue (2000). The results using monotonic fourth-order diffusion are similar to results with the standard scheme, and thus are not shown here. The results for the monotonic sixth-order scheme are shown in Fig. 13. The updraft patterns are generally smoother than in simulations without the monotonic limiter. Furthermore, the spectra for these simulations do not show any obviously unphysical patterns, and the peak at ~7Δ is no longer present (not shown).

These results provide additional support to the argument that spurious perturbations introduced by numerical schemes play a role in the development of the spurious updraft problem.

As a general rule, the simple monotonic flux limiter of Xue (2000) is recommended for simulations of mesoscale convective systems that require artificial diffusion.

c. Monotonic advection

If horizontal advection is primarily responsible for introducing spurious perturbations into the MAUL, it is reasonable to conclude that the use of a monotonic advection scheme could largely prevent the problem. Furthermore, by limiting the introduction of spurious perturbations, a numerical model might not require enhanced diffusion from turbulence schemes or from artificial diffusive terms. To this end, some monotonic advection schemes were tested on this case. Here, results are presented using the weighted essentially non-oscillatory (WENO) advection scheme of Shu (2001). This scheme is applied only to the scalar fields: i.e., potential temperature, all water mixing ratios, and turbulence kinetic energy. The advection of momentum uses the same fifth-order advection scheme as in all other simulations. Otherwise, the model is configured exactly as in the "control" simulations.

The results using WENO advection of scalars (Fig. 14) could be considered satisfactory, under the loose constraints of the qualitative assessment used in this study. Specifically, the spurious pattern is not evident, and no obviously spurious features are present in the spectra of these results (not shown). On the other hand, the updrafts are poorly resolved, as in the "control" and "shifted-wind" simulations.

Two benefits of using this monotonic advection are notable, based on this cursory study. First, the simulations with monotonic advection retain a higher effective resolution than simulations with diffusion increased via the subgrid model or via an artificial term. This factor offsets the additional cost of the scheme, which is the most expensive of all configurations

studied in this paper. Second, this monotonic scheme does not require a user-determined turbulence parameter or diffusion coefficient that needs to be set carefully based on trial and error. This property makes the scheme attractive for use in environmental sensitivity studies.

6. Conclusions

This study analyzed a spurious updraft pattern that can occur in numerical simulations of squall lines. The problem was previously documented by TR03 for the case of no environmental wind shear. This new study investigated a broader range of environmental shear conditions, and proposed an explanation for the ultimate cause of the problem. The main conclusions reached by this study are:

- The spurious pattern only occurs in certain environments. For the cases studied here, the pattern was found only in upshear-tilted convective systems.
- A lack of diffusion is not ultimately responsible for the spurious pattern. In simulations in which the model's implicit diffusion is reduced, the spurious pattern does not occur.
- The ultimate cause of the spurious pattern is the presence of statically unstable layers (i.e., MAULs) and the introduction of spurious perturbations into these layers by numerical schemes.

Typically, the atmosphere is statically stable. Thus, for most model applications, the introduction of spurious perturbations by numerical schemes does not become a serious problem, because the perturbations naturally decay. The simulation of convective systems containing

deep, broad MAULs appears to be a special circumstance that requires additional vigilance by numerical model designers and users.

This study also explored possible model formulations that can be used to diffuse and/or avoid the spurious pattern. This analysis was not exhaustive, but instead was included to illustrate how knowledge of the spurious pattern's cause can be used to evaluate numerical techniques. The conclusions reached in this part of the study include:

- The method advocated by TR03 – i.e., increased diffusion via the model's subgrid turbulence scheme – has an environmental dependence. This property makes the technique difficult to use as a general solution to the problem.
- The use of standard high-order diffusion schemes is problematic in some conditions because these schemes can introduce spurious small-scale perturbations. The addition of a monotonic limiter, such as that of Xue 2000, was found to be helpful.
- The use of a monotonic advection scheme on scalars prevented the appearance of spurious updraft patterns, although the updrafts remained poorly resolved.

The simulations in the last section of this study generally support the hypothesis from the first part. That is, simulations with numerical schemes that introduce spurious perturbations are more susceptible to the spurious updraft pattern.

The lack of a definitive benchmark solution prevents an assessment of what is the best model configuration. However, as noted in TR03, several obviously bad model configurations have been noted. What can be concluded with certainty is that squall line simulations with low shear conditions are more sensitive to model formulation than simulations with high shear

conditions. Because of this sensitivity, more careful model setup is necessary for simulations of upshear-tilted convective systems.

Simulations with 125 m grid spacing are currently being conducted for the $U_s = 0$ m s^{-1} environment. It is hoped that the higher resolution runs will lead to a benchmark solution, which could be used to revisit the issue of best model formulation with *O*(1 km) grid spacing. However, preliminary results indicate that the high-resolution runs are also sensitive to model formulation. This result is not surprising. A deep, wide MAUL still exists with high resolution, and the overturning of this layer is still sensitive to how it is perturbed by necessarily imperfect numerical schemes. At this time, a benchmark solution remains elusive.

Acknowledgments

I would like to acknowledge fruitful discussions on this topic with Rich Rotunno, Jason Knievel, Matt Parker, Tetsuya Takemi, and Richard James. This work was supported by the Advanced Study Program of NCAR. All figures were created using the Grid Analysis and Display System (GrADS).

References

Bryan, G. H., and J. M. Fritsch, 2000: Moist absolute instability: The sixth static stability state. *Bull. Amer. Meteor. Soc.,* **81,** 1207-1230.

——, and ——, 2002: A benchmark simulation for moist nonhydrostatic numerical models. *Mon. Wea. Rev.,* **130**, 2917-2928.

——, J. C. Wyngaard, and J. M. Fritsch, 2003: Resolution requirements for the simulation of deep moist convection. *Mon. Wea. Rev.*, **131**, 2394-2416.

Carpenter, R. L., Jr., K. K. Droegemeier, and A. M. Blyth, 1998: Entrainment and detrainment in numerically simulated cumulus congestus clouds. Part I: General results. *J. Atmos. Sci.,* **55**, 3417-3432.

Deardorff, J. W.,, 1980: Stratocumulus-capped mixed layer derived from a three-dimensional model. *Bound.-Layer Meteor.,* **18**, 495-527.

Dudhia, J., 1993: A nonhydrostatic version of the Penn State-NCAR Mesoscale Model: Validation tests and simulation of an Atlantic cyclone and cold front. *Mon. Wea. Rev.,* **121,** 1493-1513.

Durran, D. R., 1999: *Numerical Methods for Wave Equations in Geophysical Fluid Dynamics.* Springer-Verlag, 465 pp.

——, and J. B. Klemp, 1982: On the effects of moisture on the Brunt-Väisälä Frequency. *J. Atmos. Sci.,* **39,** 2152-2158.

Kain, J. S., and J. M. Fritsch, 1998: Multiscale convective overturning in mesoscale convective systems: Reconciling observations, simulations, and theory. *Mon. Wea. Rev.,* **126,** 2254-2273.

Kessler, E., 1969: *On the Distribution and Continuity of Water Substance in Atmospheric Circulation, Meteor. Monogr.,* No. 32, Amer. Meteor. Soc., 84 pp.

Klemp, J. B., and R. B. Wilhelmson, 1978: The simulation of three-dimensional convective storm dynamics. *J. Atmos. Sci.,* **35,** 1070-1096.

Lane, T. P., R. D. Sharman, T. L. Clark, and H.-M. Hsu, 2003: An investigation of turbulence generation mechanisms above deep convection. *J. Atmos. Sci.,* **60,** 1297-1321.

Mason, P. J., and A. R. Brown, 1999: On subgrid models and filter operations in large eddy simulation. *J. Atmos. Sci.,* **56,** 2101-2114.

Rotunno, R., J. B. Klemp, and M. L. Weisman, 1988: A theory for strong, long-lived squall lines. *J. Atmos. Sci.,* **45**, 463-485.

Shu, C.-W., 2001: High order finite difference and finite volume WENO schemes and discontinuous Galerkin methods for CFD. ICASE Report No. 2001-11, 16 pp. [Available from NASA Langley Research Center, Hampton, VA, 23681-2199.]

Skamarock, W. C., 2004: Evaluating mesoscale NWP models using kinetic energy spectra. Submitted to *Mon. Wea. Rev.,* March 2004.

Takemi, T., and R. Rotunno, 2003: The effects of subgrid model mixing and numerical filtering in simulations of mesoscale cloud systems. *Mon. Wea. Rev.,* **131,** 2085-2101.

Weisman, M. L., 1993: The genesis of severe, long-lived bow echoes. *J. Atmos. Sci.,* **50,** 645-670.

——, and J. B. Klemp, 1982: The dependence of numerically simulated convective storms on vertical wind shear and buoyancy. *Mon. Wea. Rev.,* **110,** 504-520.

——, ——, and R. Rotunno, 1988: Structure and evolution of numerically simulation squall lines. *J. Atmos. Sci.,* **45,** 1990-2013.

Wicker, L. J., and W. C. Skamarock, 2002: Time splitting methods for elastic models using forward time schemes. *Mon. Wea. Rev*., **130**, 2088-2097.

Xue, M., 2000: High-order monotonic numerical diffusion and smoothing. *Mon. Wea. Rev.,*

128, 2853-2864.

——, M., K. K. Droegemeier, and V. Wong, 2000: The Advanced Regional Prediction System (ARPS) – A multiscale nonhydrostatic atmospheric simulation and prediction model. Part I: Model dynamics and verification. *Meteor. Atmos. Phys.,* **75,** 161-193.

Table Captions

Table 1. Approximate coefficients of diffusion ($\times 10^{-5}$ s^{-1}) for simulations in which the squall line remains near the center of the domain ("control"), and for simulations in which the mean wind is nearly zero in the region of interest ("shifted-wind").

Table 2. Average statistics (3-4 h) for 80 parcels (released every 1 km in *y* at 1.25 km above ground) in the "control" simulations.

Table 3. The same as in Table 2, except for the "shifted-wind" simulations.

Table 1. Approximate coefficients of diffusion ($\times 10^{-5}$ s^{-1}) for simulations in which the squall line remains near the center of the domain ("control"), and for simulations in which the mean wind is nearly zero in the region of interest ("shifted-wind").

U_s (m s^{-1})	Control	Shifted-wind
0	8.9	0.8
10	23.6	0.4
20	21.1	0
30	8.6	3.5

Table 2. Average statistics (3-4 h) for 80 parcels (released every 1 km in *y* at 1.25 km above ground) in the "control" simulations.

U_s (m s^{-1})	Average time within MAUL (min)	Average horizontal (*x*) displacement within MAUL (km)
0	14.4	4.5
10	9.5	6.8
20	9.9	7.5
30	7.8	2.5

Table 3. The same as in Table 2, except for the "shifted-wind" simulations.

U_s (m s^{-1})	Average time within MAUL (min)	Average horizontal (*x*) displacement within MAUL (km)
0	14.4	0.9
10	13.2	1.8
20	10.2	2.2
30	7.8	2.4

Figure Captions

Fig. 1. Vertical velocity (m s^{-1}) at 3 km above ground and 3 h from a simulation of a squall line with no environmental wind shear. Contour interval is 1 m s^{-1} with negative contours dashed and the zero contour excluded. The thick dashed contour is the position of the surface gust front.

Fig. 2. Initial conditions for the squall line simulations. (a) Initial thermodynamic conditions. (b) Initial wind profiles.

Fig. 3. Vertical velocity at 3 km and 4 h from simulations with (a) $U_s = 0$, (b) $U_s = 10$, (c) $U_s = 20$, (d) $U_s = 30$ m s^{-1}. The contour interval is 1 m s^{-1} for panel (a), and is 2 m s^{-1} for all other panels, with negative contours dashed and the zero contour excluded. The thick dashed contour is the position of the surface gust front.

Fig. 4. The same as in Fig. 3, except for "shifted-wind" simulations, in which the mean horizontal (x) flow at this level is approximately zero near the updrafts.

Fig. 5. Vertical velocity spectra at 3 km for "control" (thick solid) and "shifted-wind" (thin solid) simulations with (a) $U_s = 0$, (b) $U_s = 10$, (c) $U_s = 20$, and (d) $U_s = 30$ m s^{-1}. The along-line spectra have been multiplied by 100 to avoid overlap. Two thick gray lines illustrating $\kappa^{-5/3}$ spectra have been included for reference. The vertical line denotes the 6Δ scale.

Fig. 6. A vertical cross section at y = 23 km and t = 4 h from the "control" simulation with U_s = 0 m s^{-1}. Equivalent potential temperature (K) is shaded. Vertical velocity is contoured with a contour interval of 1 m s^{-1}, negative contours dashed, and the zero contour excluded.

Fig. 7. A sounding at x = 313 km, y = 23 km, and t = 4 h from the control simulation with U_s = 0 m s^{-1}.

Fig. 8. A time-space (i.e., Hovmöller diagram) of vertical velocity (m s^{-1}) at y = 39 km and z = 3 km from the control simulation with U_s = 0 m s^{-1}.

Fig. 9. Line-averaged plots of equivalent potential temperature (K) from "control" simulations with (a) U_s = 0, (b) U_s = 10, (c) U_s = 20, and (d) U_s = 30 m s^{-1}. The dashed contour encloses regions in which more that 50% of the volume is moist absolutely unstable. Sample parcel trajectories are shown by thick solid lines. The parcels trajectories begin at z = 1.75 km and ~10-20 km east of the squall lines.

Fig. 10. Vertical velocity at 3 km and 4 h from simulations with C_k = 0.20 using (a) U_s = 0, and (b) U_s = 10 m s^{-1} environments. The contouring is the same as in Fig. 3.

Fig. 11. The same as in Fig. 10, except for simulations with regular fourth-order diffusion.

Fig. 12. The same as in Fig. 10, except for simulations with regular sixth-order diffusion.

Fig. 13. The same as in Fig. 10, except for simulations with monotonic sixth-order diffusion.

Fig. 14. The same as in Fig. 10, except for simulations with WENO advection on scalars.

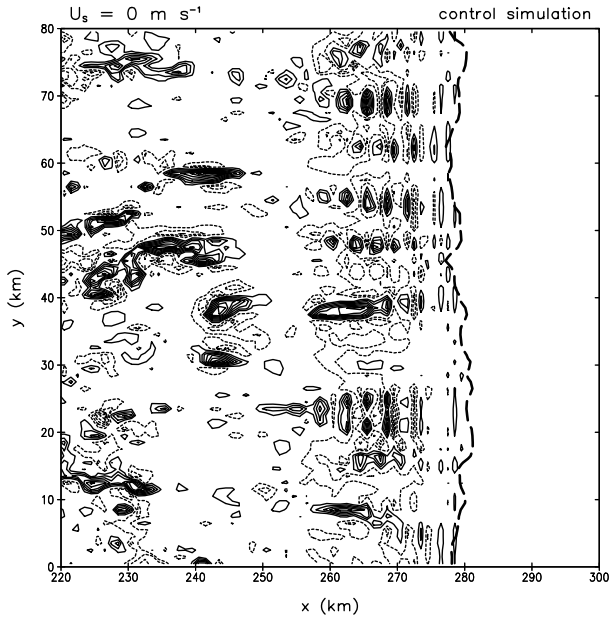

Fig. 1. Vertical velocity (m s^{-1}) at 3 km above ground and 3 h from a simulation of a squall line with no environmental wind shear. Contour interval is 1 m s^{-1} with negative contours dashed and the zero contour excluded. The thick dashed contour is the position of the surface gust front.

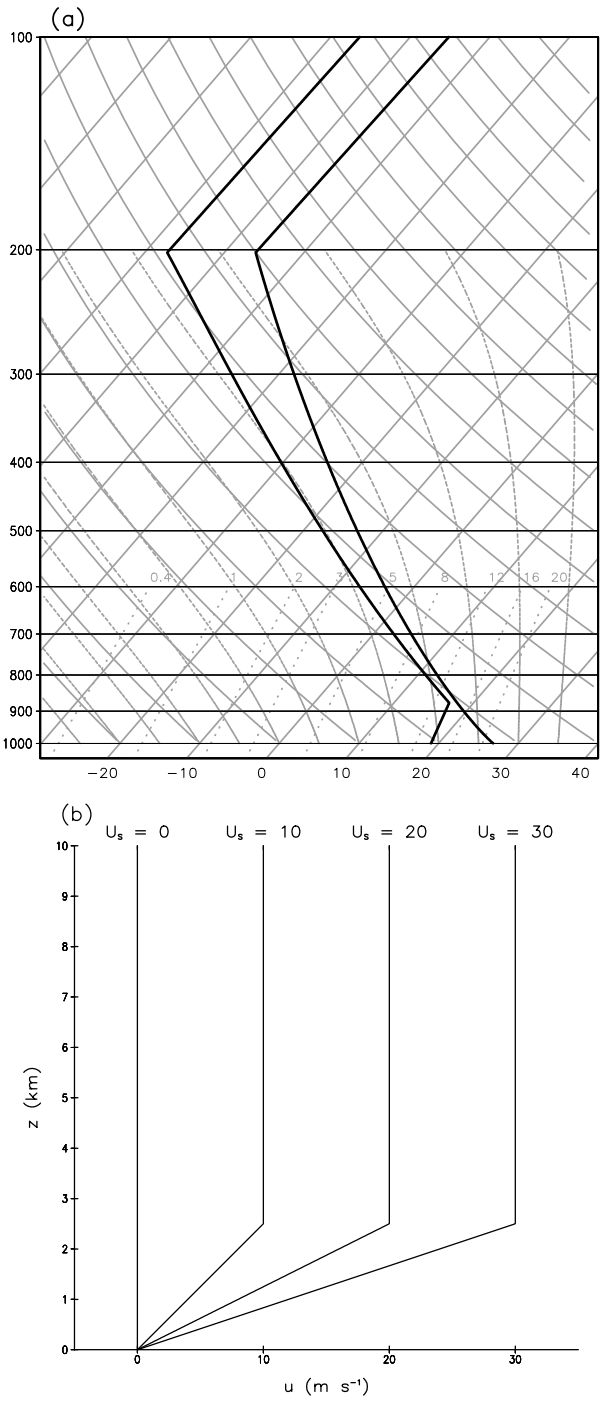

Fig. 2. Initial conditions for the squall line simulations. (a) Initial thermodynamic conditions. (b) Initial wind profiles.

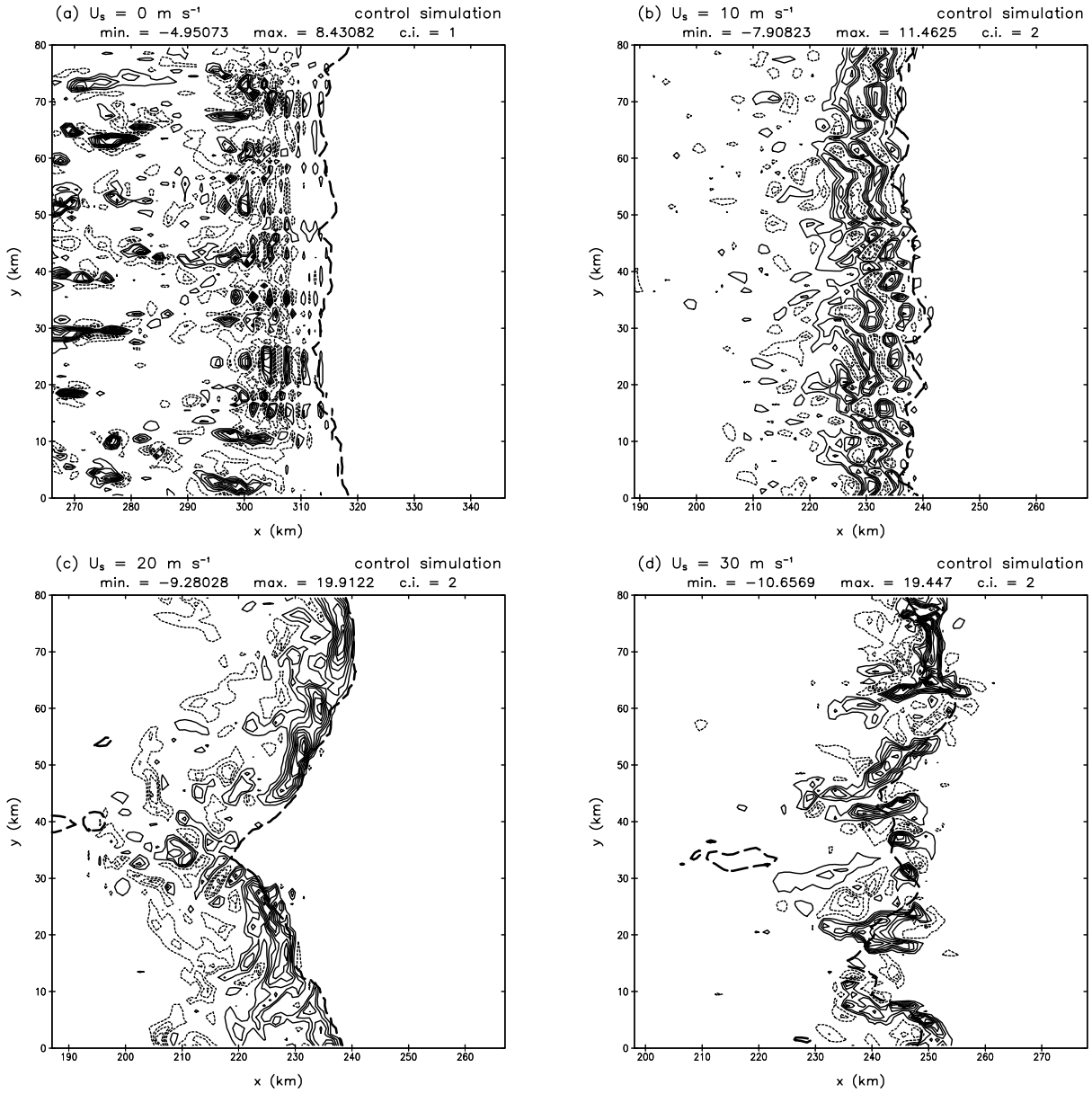

Fig. 3. Vertical velocity at 3 km and 4 h from simulations with (a) $U_s = 0$, (b) $U_s = 10$, (c) $U_s = 20$, (d) $U_s = 30$ m s^{-1}. The contour interval is 1 m s^{-1} for panel (a), and is 2 m s^{-1} for all other panels, with negative contours dashed and the zero contour excluded. The thick dashed contour is the position of the surface gust front.

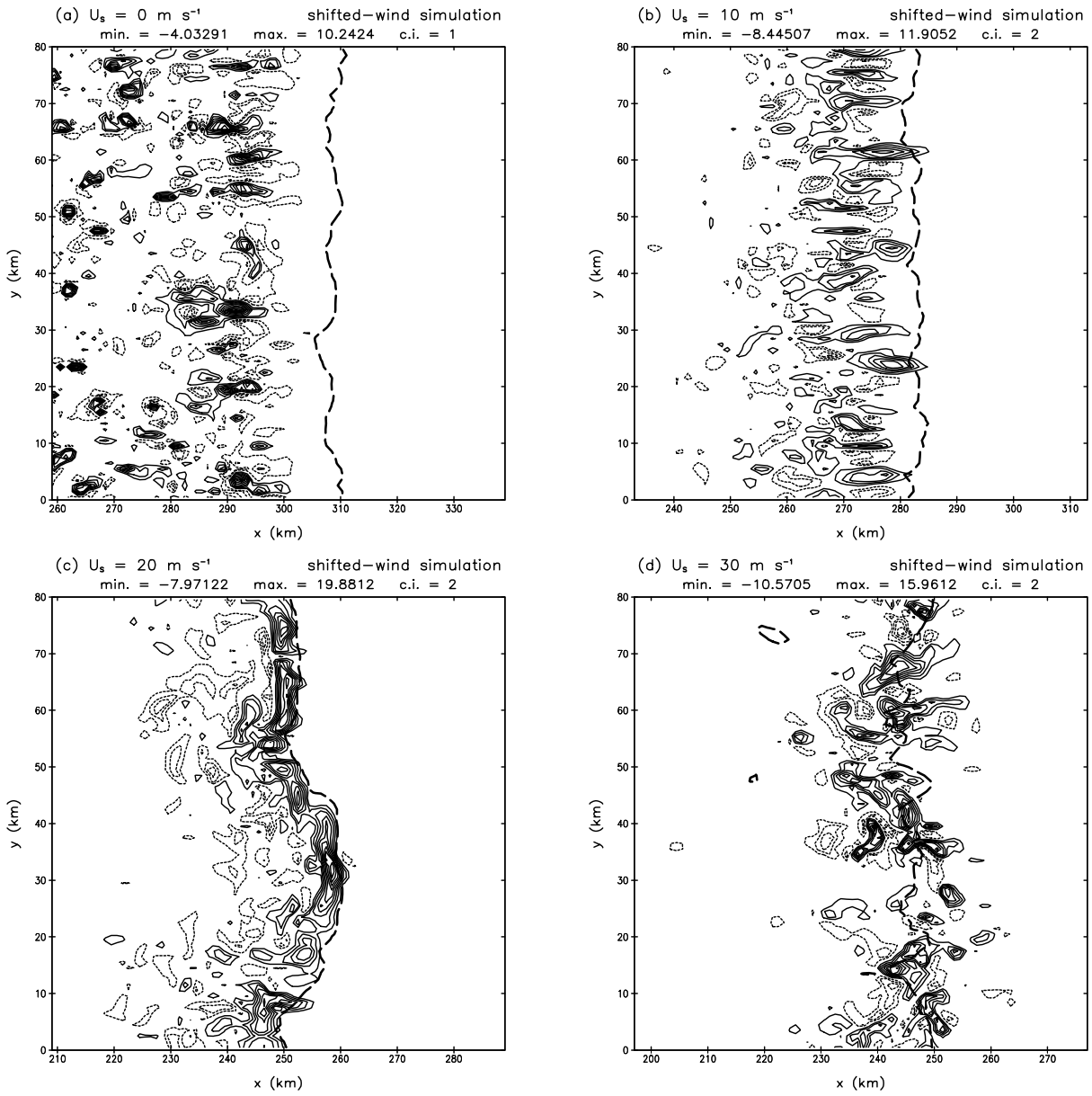

Fig. 4. The same as in Fig. 3, except for "shifted-wind" simulations, in which the mean horizontal (x) flow at this level is approximately zero near the updrafts.

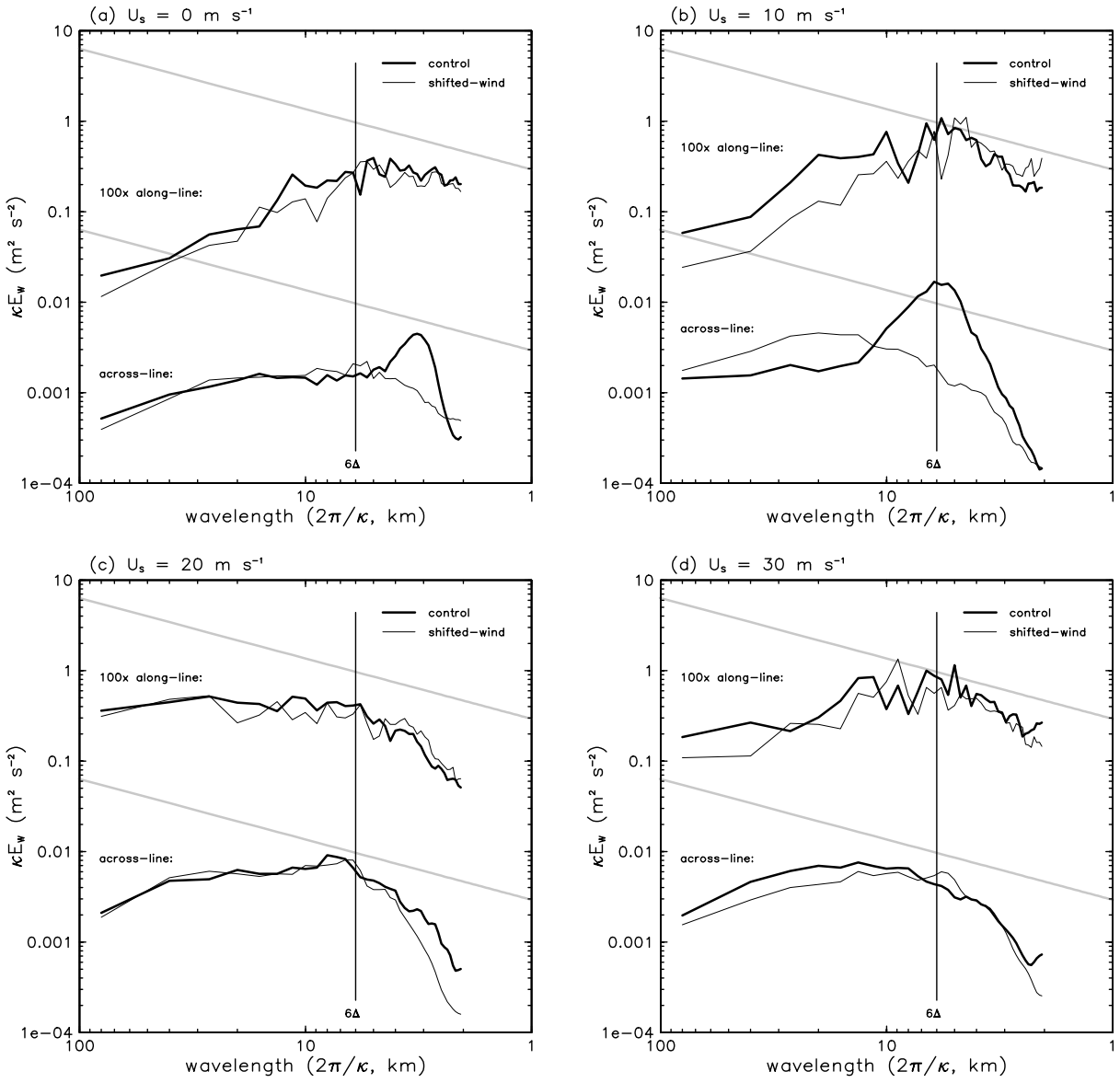

Fig. 5. Vertical velocity spectra at 3 km for "control" (thick solid) and "shifted-wind" (thin solid) simulations with (a) $U_s = 0$, (b) $U_s = 10$, (c) $U_s = 20$, and (d) $U_s = 30$ m s^{-1}. The along-line spectra have been multiplied by 100 to avoid overlap. Two thick gray lines illustrating $\kappa^{-5/3}$ spectra have been included for reference. The vertical line denotes the 6Δ scale.

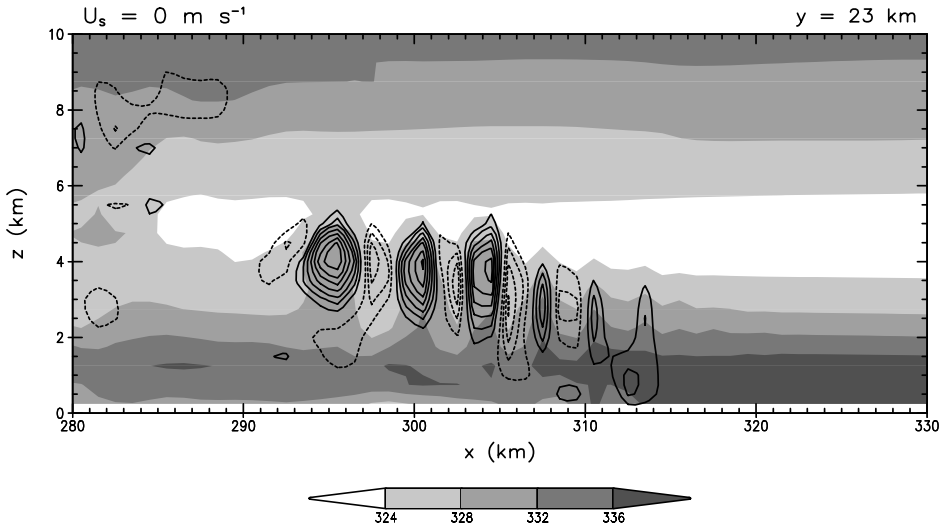

Fig. 6. A vertical cross section at y = 23 km and t = 4 h from the "control" simulation with U_s = 0 m s^{-1}. Equivalent potential temperature (K) is shaded. Vertical velocity is contoured with a contour interval of 1 m s^{-1}, negative contours dashed, and the zero contour excluded.

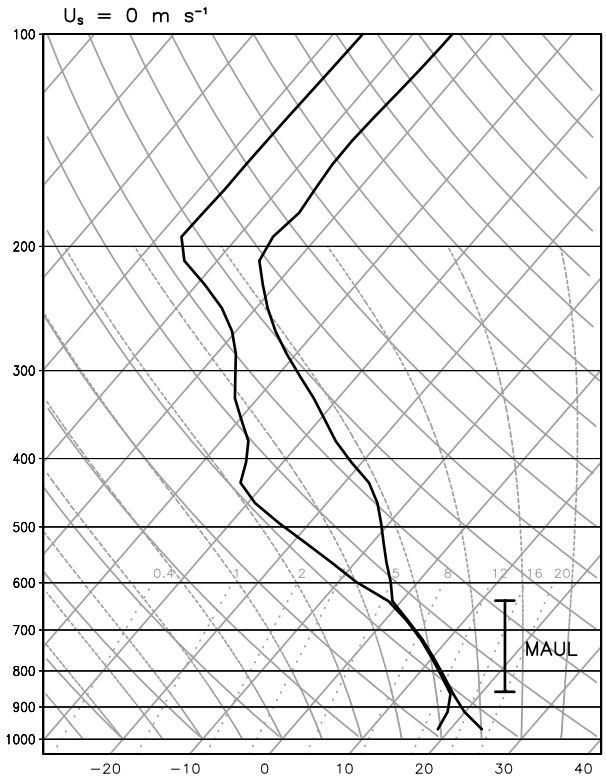

Fig. 7. A sounding at x = 313 km, y = 23 km, and t = 4 h from the control simulation with U_s = 0 m s^{-1}.

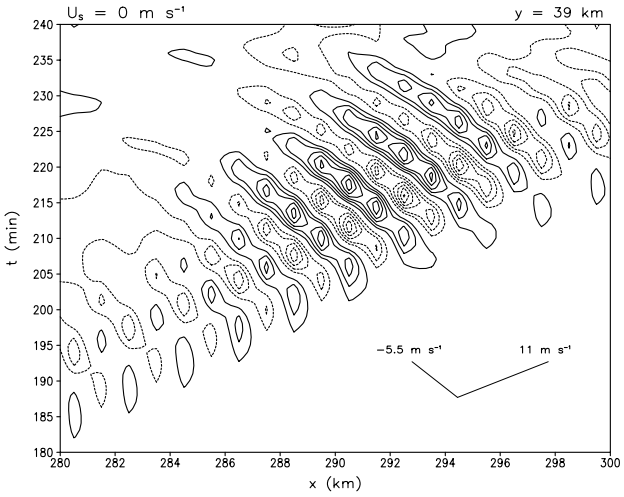

Fig. 8. A time-space (i.e., Hovmöller diagram) of vertical velocity (m s^{-1}) at y = 39 km and z = 3 km from the control simulation with U_s = 0 m s^{-1}.

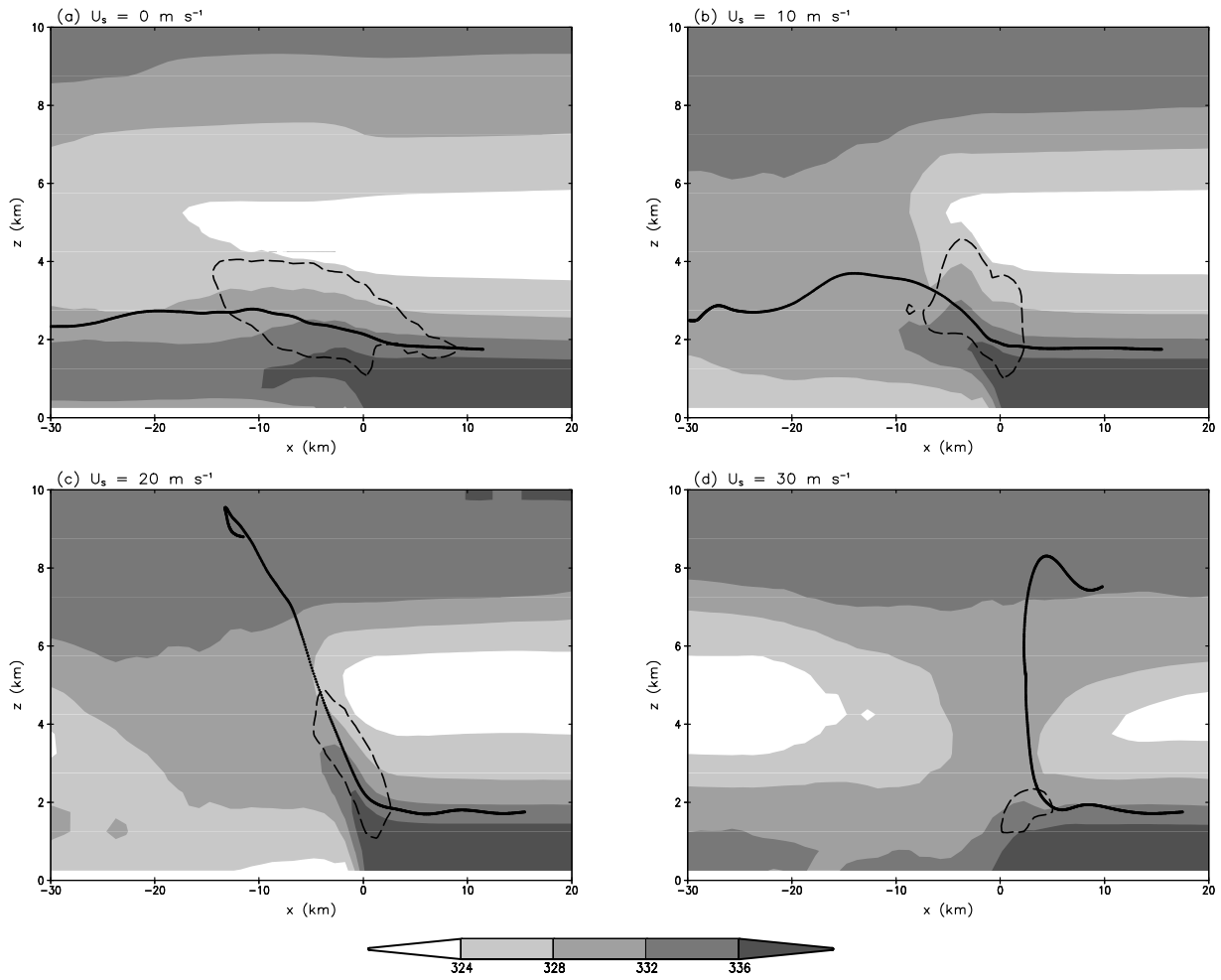

Fig. 9. Line-averaged plots of equivalent potential temperature (K) from "control" simulations with (a) $U_s = 0$, (b) $U_s = 10$, (c) $U_s = 20$, and (d) $U_s = 30$ m s^{-1}. The dashed contour encloses regions in which more that 50% of the volume is moist absolutely unstable. Sample parcel trajectories are shown by thick solid lines. The parcels trajectories begin at $z = 1.75$ km and ~10-20 km east of the squall lines.

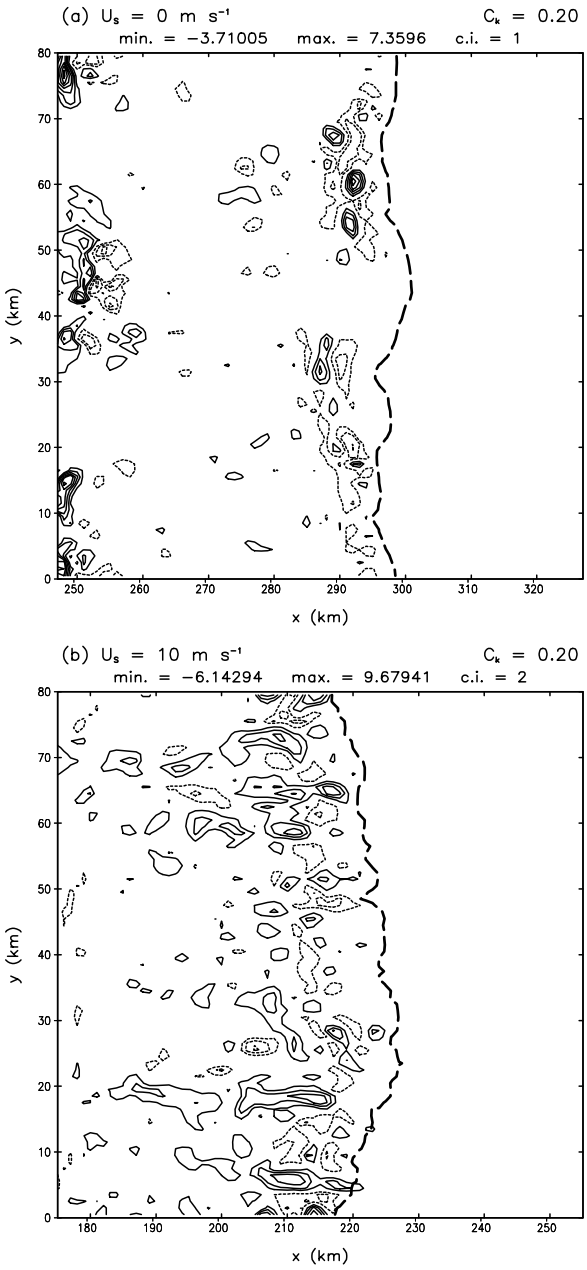

Fig. 10. Vertical velocity at 3 km and 4 h from simulations with C_k = 0.20 using (a) U_s = 0, and (b) U_s = 10 m s^{-1} environments. The contouring is the same as in Fig. 3.

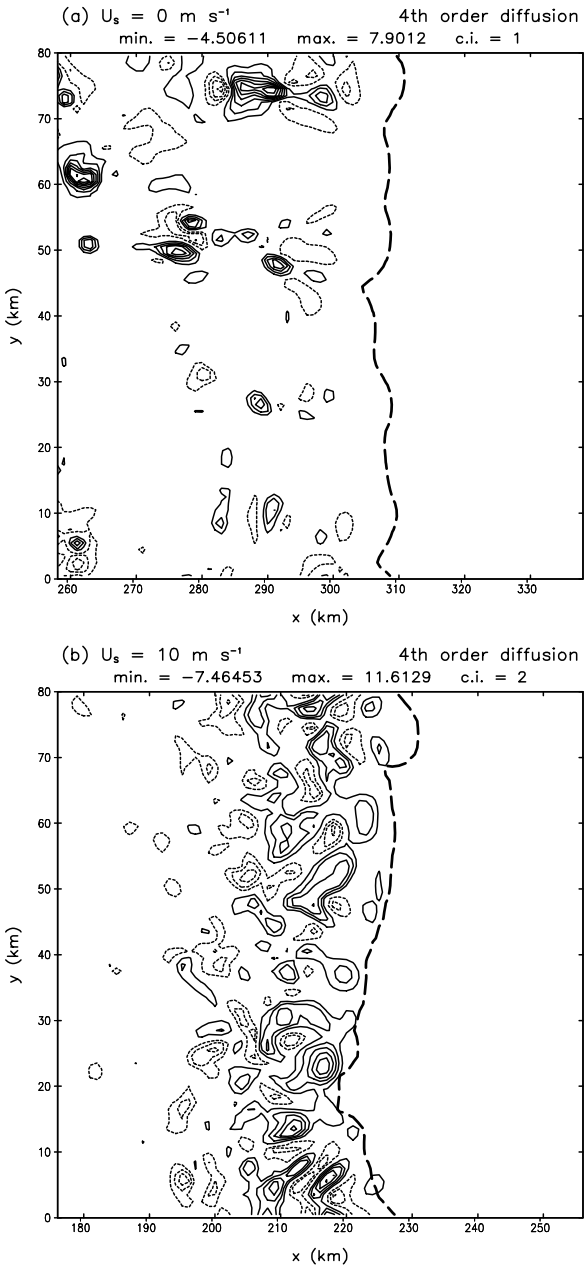

Fig. 11. The same as in Fig. 10, except for simulations with regular fourth-order diffusion.

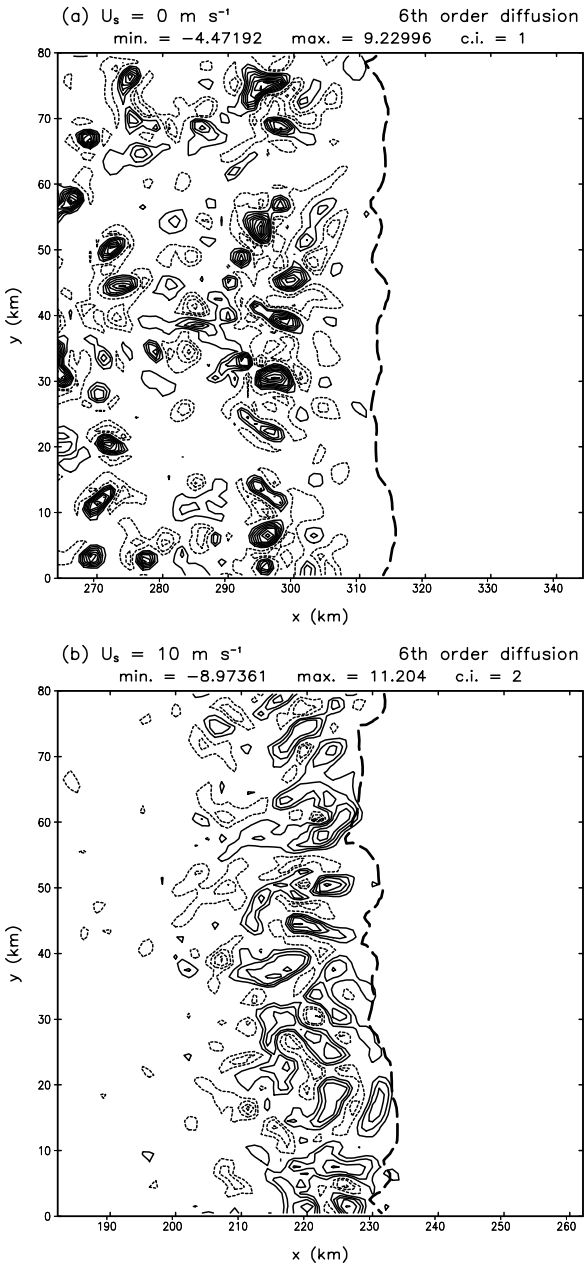

Fig. 12. The same as in Fig. 10, except for simulations with regular sixth-order diffusion.

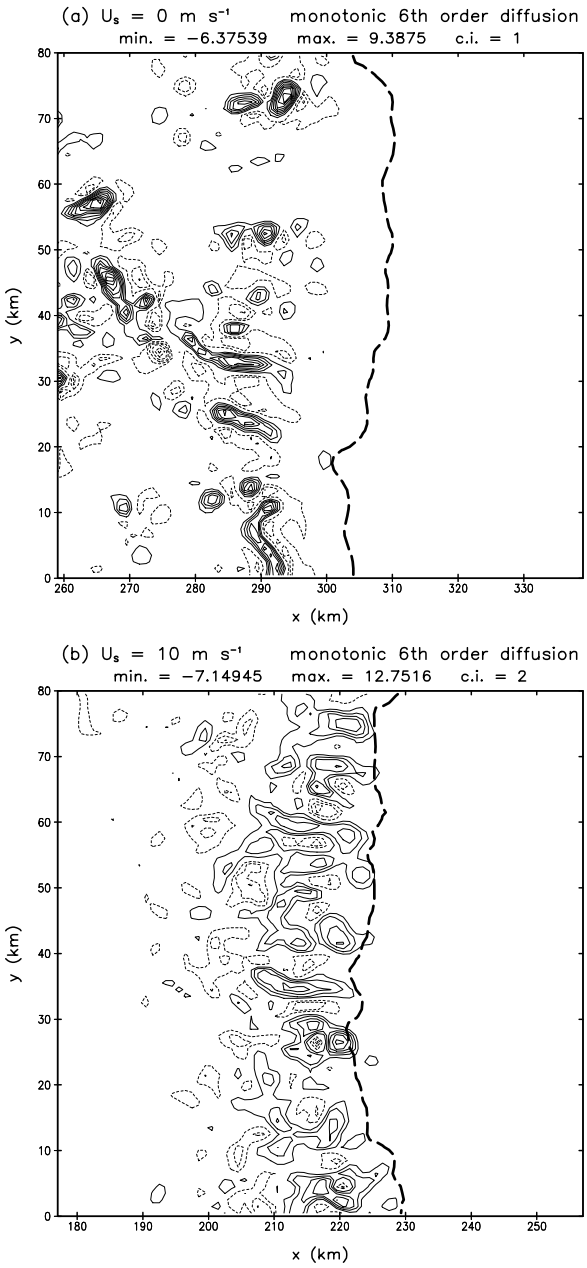

Fig. 13. The same as in Fig. 10, except for simulations with monotonic sixth-order diffusion.

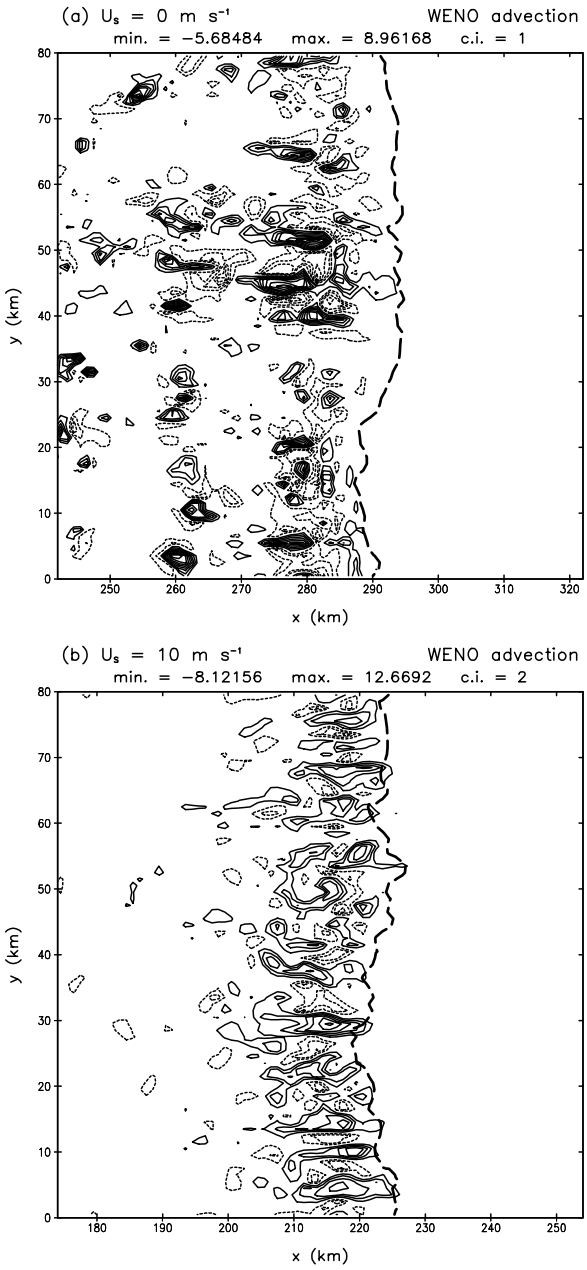

Fig. 14. The same as in Fig. 10, except for simulations with WENO advection on scalars.